Test and optimization of a multi-modal phase-based x-ray microscope for soft tissue imaging

Esposito, M., Massimi, L., Buchanan, I., Ferrara, J., Endrizzi, M., et al.

M. Esposito, L. Massimi, I. Buchanan, J. D. Ferrara, M. Endrizzi, A. Olivo, "Test and optimization of a multi-modal phase-based x-ray microscope for soft tissue imaging," Proc. SPIE 12031, Medical Imaging 2022: Physics of Medical Imaging, 1203102 (4 April 2022); doi: 10.1117/12.2609441

SPIE.

Event: SPIE Medical Imaging, 2022, San Diego, California, United States

Test and optimisation of a multi-modal phase-based x-ray microscope for soft tissue imaging.

M. Esposito[1], L. Massimi[1], I. Buchanan[1], J. D. Ferrara[2], M. Endrizzi[1], and A. Olivo[1]

[1]*Department of Medical Physics and Biomedical Engineering, University College London, Gower St, London WC1E 6BT, UK*

[2]*Rigaku Americas Corporation, 9009 New Trails Drive, The Woodlands, Texas 77381, US*

Introduction

Tissue imaging is a pivotal component of both biomedical research and clinical practice. In order to identify tissue structures down to the cellular level, it requires the capability to image millimiter size unstained tissue specimens with micron to sub-micron resolution. Tissue imaging is normally performed either using x-rays or visible light. While the latter is limited by light scattering in relatively thick tissues, the former often suffers from poor contrast in absorption-based systems. Phase-contrast x-ray microscopes exist but they often lack the required quantitativeness, entail acquisition times of the order of tens of hours for 3D imaging and are limited to narrow fields of view (which can be <100 μm) [1, 2].

We propose a novel multi-modal phase-based x-ray microscope capable of imaging mm-thick tissue samples on a mm-size field of view through the use of intensity-modulation masks. They act as optical elements allowing the quantitative retrieval of tissue properties such as transmission, refraction and ultra-small angle scattering or dark field. Additionally, given that the system's spatial resolution depends only on the mask aperture size [3], a multi-resolution approach is possible by selecting masks with aperture size matching the resolution requirements of specific samples.

We report on an investigation of the parameter space for the x-ray microscope and provide exemplar images of its applications to materials and life science, showing the complementarity of the contrast channels for a foam sample and beetle leg.

Materials and Methods

The laboratory setup consists of a rotating-anode (Cu) X-ray generator coupled to a doubly curved multi-layer monochromator selecting the Cu Kα emission line [4] which also focuses the beam to a 350 μm focal spot, an intensity-modulation mask and a detector. A schematic diagram of the set-up is shown in Figure 1. The intensity-modulation mask, featuring periodic apertures in the direction perpendicular to that of the system sensitivity, shapes the x-ray beam into an array of beamlets. Modifications in the shaped beamlets due to the presence of a sample allow for the retrieval of the sample properties. Two different pre-sample masks were tested in this work, with periods P_1=9.5

Medical Imaging 2022: Physics of Medical Imaging, edited by Wei Zhao, Lifeng Yu, Proc. of SPIE
Vol. 12031, 1203102 · © 2022 SPIE · 1605-7422 · doi: 10.1117/12.2609441

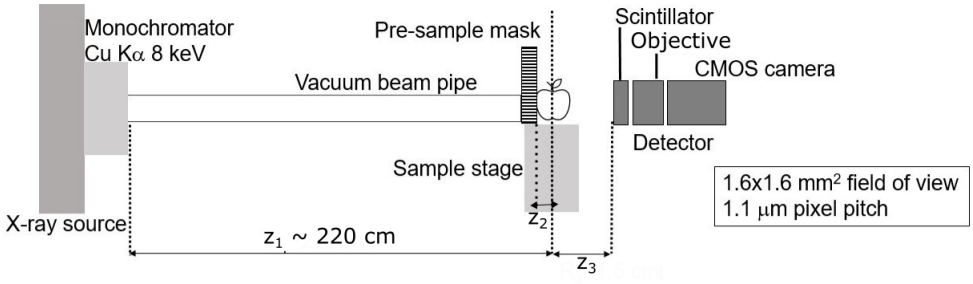

Figure 1: A schematic diagram of the phase-based x-ray microscope.

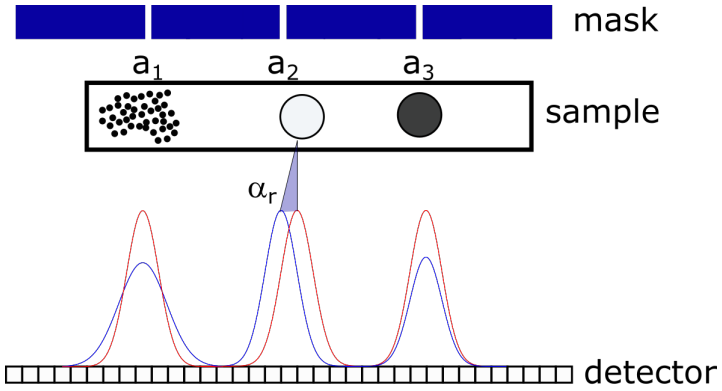

Figure 2: A schematic diagram of the beam tracking retrieval method. The red curve shows the shaped beamlets in absence of a sample.These are modified into the blue curve when a sample is placed between mask and detector.

μm and P_2=19 μm and aperture width w=2 μm in both cases. Both masks were fabricated by Microworks GmbH (Karlsruhe, Germany) on a free-standing 20 μm thick Au layer. Masks were placed 2.2 m away from the source. A propagation distance of 15 mm was allowed between pre-sample mask and detector, which consists of a scintillator focused on a scientific CMOS camera leading to an effective pixel pitch of 1.1μm and a 1.6×1.6 mm^2 field of view.

Retrieval of three contrast channels - namely transmission, refraction and ultra-small angle scattering (or dark field) - was performed using the so-called *beam tracking* approach [5, 6], which had previously only been used with much higher energy x-rays. A schematic representation of the working principle underlying the beam tracking approach and the retrieval method is shown in Figure 2. The x-ray beam is shaped into an array of beamlets by the intensity-modulation mask, generating a signal represented by the red curve in Figure 2. Introducing a sample, between mask and detector, produces a number of modifications in the shaped beamlets. For ease of representation, the sample is considered to be made of three separate purely scattering, purely refracting and purely

absorbing regions labelled as a_1, a_2 and a_3, respectively. The beamlets recorded by detector with the sample in place are represented by the blue curve. Scattering leads to a broadening of the shaped beamlet, refraction to a displacement determined by the refraction angle α_r, and absorption to a reduction in the amplitude of the beamlet. Indicating with $[A, \mu, \sigma^2]$ amplitude, mean and variance of each beamlet, transmission (T), refraction (R) and scattering (S) can be retrieved as follows:

$$T = \frac{A'}{A} \tag{1}$$

$$R = \frac{\mu' - \mu}{z_3} \tag{2}$$

$$S = \frac{\sigma'^2 - \sigma^2}{z_3^2} \tag{3}$$

where the prime symbol is used to indicate beamlet parameters when the sample is in place and z_3 is the distance between sample and detector.

In order to explore the parameters space of the x-ray microscope, numerical simulation based on the Fresnel–Kirchoff theory of diffraction in the Fresnel approximation [7] were performed. The gold intensity-modulation mask was modelled using nominal parameters for thickness (20 μm) and aperture width (2 μm), while the period varied in the range 2 to 28 μm. The detector pixel pitch was assumed to be 1.1 μm with a Point Spread Function (PSF) Full-Width-at-Half-Maximum (FWHM) of 1.5 μm. Source size and mask-to-detector distance were varied in the range 1μm to 1 mm and 5 mm to 50 mm, respectively. For each simulation point the visibility of the beamlets, as seen by the detector, was calculated as

$$V = \frac{I_{max} - I_{min}}{I_{max} + I_{min}} \tag{4}$$

with I_{max} and I_{min} corresponding to the intensity of peaks and valleys of the shaped beamlets, respectively.

An approximately 1-mm thick foam sample and a dried beetle leg were imaged with the x-ray microscope with the P_2 mask and a $z_3 = 15$ mm.

Results

Figure 3 *a)* and 3 *b)* show the simulated visibility of the shaped beamlets as a function of source size and ratio of period to mask aperture (P/w) for a fixed mask-to-detector distance z_3 of 15 mm, and as function of source size and mask-to-detector distance for a fixed mask period of 20 μm, respectively. The visibility decreases with decreasing mask period and increasing source size, approaching zero for the shortest periods considered in this study when the source size is small (< 200 μm), and for periods up to several times the aperture width for larger source sizes. The visibility also has a dependence on z_3, and it decreases with increasing z_3 for source sizes greater than 400 μm.

An image of the two pre-sample masks is reported in Figure 4, with masks of period P_1=9.5 μm and P_2=19 μm shown in panels *a)* and *b)*, respectively. A comparison of the intensity profiles shows how the longer period mask (P_2) leads to a higher visibility of the shaped beamlets. Differences in visibility, arising from tuning of the mask period, source size and propagation distance, have an effect on the retrieval procedure of some of the contrast channels (scattering and transmission), as well as

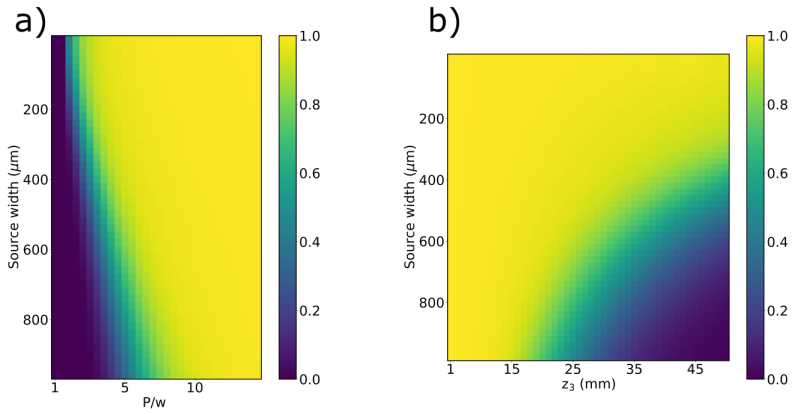

Figure 3: Simulated visibility as defined in eq. 4 as a function of the ratio of mask to aperture period (P/w) and source size *a)*, and of propagation distance and source size *b)*.

on the Signal-to-Noise Ratio (SNR) of the acquired images. A higher offset and a smaller separation between beamlets (as in Figure 4 *a)*) results in an increased uncertainty in the estimation of the tails of the beamlets. This translates in an increased uncertainty in the estimation of their width and amplitude and, therefore, in the scattering and transmission signals. A longer propagation distance contributes to the broadening of the beamlets, so that an increased photon flux is needed to preserve the same number of counts per detector pixel compared to narrower beamlets.

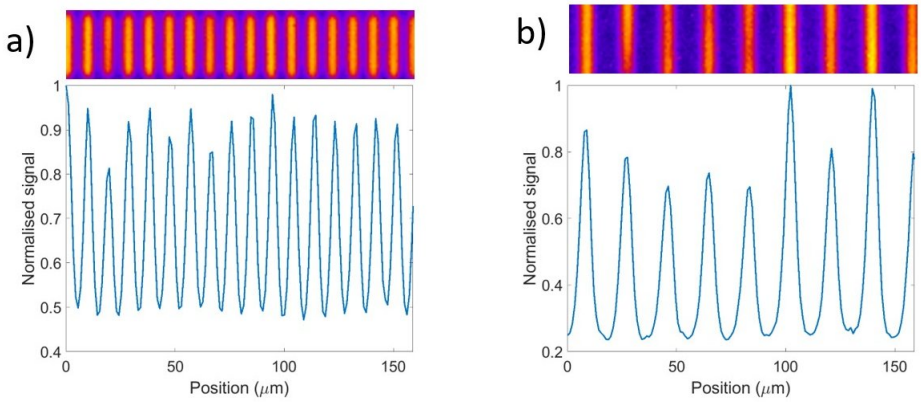

Figure 4: Images of a small region (160×32 μm^2) of the pre-sample mask and corresponding row profiles across the apertures for the masks with period P1=9.5 μm *a)* and with P2=19 μm *b)*.

Figure 5 shows the retrieved transmission *a)*, refraction *b)*, scattering *c)* and integrated phase *d)* for a 1-mm thick foam layer. Phase integration was performed using the algorithm presented in [8]. While some thickness variations are visible in the transmission image, the microscopic structure

of the sample (at length scale of a few μm) is visible much more clearly in the refraction and integrated phase images of panels *b)* and *d)*. In all these images the resolution is determined by the size of the mask aperture (2 μm), possibly with some small blurring in *d)* caused by the use of the Wiener filtration as required by the algorithm described in [8]. Due to the lack of structures below the 2 μm resolution, no signal is expected in the scattering image *c)* with the exception of an edge-enhancement effect.

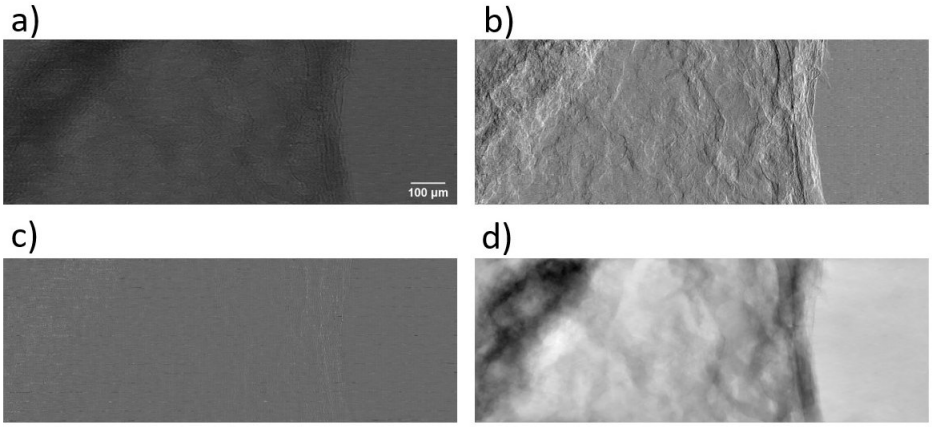

Figure 5: Transmission *a)*, refraction *b)*, scattering *c)* and integrated phase *d)* using the algorithm presented in [8] for a thin foam layer.

Retrieved images for transmission *a)*, refraction *b)* and scattering *c)* of a region of a beetle leg are shown in Figure 6. Red arrows highlight details visible in the refraction and scattering images, but not detectable in transmission, demonstrating the increased contrast of weakly absorbing samples when imaged with this phase-based imaging modality. A magnified view of the region, indicated by the red square, is shown in panels *d)*, *e)* and *f)* for transmission, refraction and scattering, respectively. The refraction and scattering images for this ROI show the edges of a vessel (identified by red arrowheads) which is not visible in the transmission image.The horizontal lines visible primarily in the attenuation and scatter images are caused by the mask apertures being periodically interrupted by gold bridges, with a consequent lack of detected photons in the affected areas. These bridges can be eliminated in future mask developments.

Conclusion

A novel multi-modal phase-based x-ray microscope for soft tissue imaging has been presented. The parameter space has been investigated and the inter-dependence of the system parameters discussed. Exemplar images for material and life science have been presented, showing the imaging capabilities of the system and the complementarity of the contrast channels.

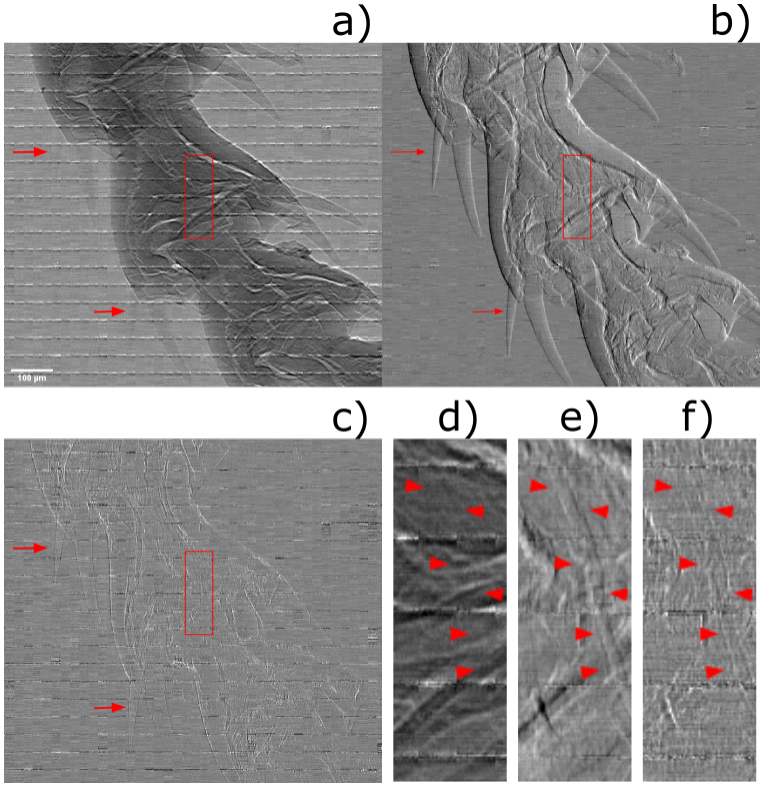

Figure 6: Transmission *a)*, refraction *b)* and scattering *c)* images of a beetle leg. The region indicated by the red square is shown magnified in panels *d)*, *e)* and *f)* for transmission, refraction and scattering. Structured noise, oriented in the direction orthogonal to the mask slits, is visible in the retrieved images. This is due to the manufacturing process of the specific mask used in this work and should not be interpreted as an intrinsic limitation of the technique. Arrows in *a)*, *b)*, *c)* indicate details clearly detected in the refraction and scattering images and hardly visible in the attenuation one. Arrowheads in *d)*, *e)*, *f)* indicate a vessel which is also invisible in attenuation but detected in the other two channels.

Acknowledgement

Research reported in this publication was supported by the National Institute of Biomedical Imaging and Bioengineering of the National Institutes of Health under Award Number R01EB028829. The content is solely the responsibility of the authors and does not necessarily represent the official views of the National Institutes of Health. Additional support was received from EPSRC (grants EP/T005408/1, EP/P023231/1 and EP/M028100/1). M.En. was supported by the Royal Academy of Engineering under the RAEng Research Fellowships scheme. AO was supported by the Royal Academy of Engineering under their "Chairs in Emerging Technologies" scheme.

Additional notes

The work presented here has not and is not being submitted for publication or presented elsewhere. However, further results resulting from the development of the x-ray microscope might be published elsewhere.

References

[1] Eastwood, D. S., Bradley, R. S., Tariq, F., Cooper, S. J., Taiwo, O. O., Gelb, J., Merkle, A., Brett, D. J. L., Brandon, N. P., Withers, P. J., Lee, P. D., and Shearing, P. R., "The application of phase contrast X-ray techniques for imaging Li-ion battery electrodes," *Nuclear Instruments and Methods in Physics Research Section B: Beam Interactions with Materials and Atoms* **324**, 118–123 (Apr. 2014).

[2] Taiwo, O. O., Finegan, D. P., Gelb, J., Holzner, C., Brett, D. J. L., and Shearing, P. R., "The use of contrast enhancement techniques in X-ray imaging of lithium–ion battery electrodes," *Chemical Engineering Science* **154**, 27–33 (Nov. 2016).

[3] Diemoz, P. C., Vittoria, F. A., and Olivo, A., "Spatial resolution of edge illumination X-ray phase-contrast imaging," *Opt. Express, OE* **22**, 15514–15529 (June 2014).

[4] Brombal, L., Kallon, G., Jiang, J., Savvidis, S., De Coppi, P., Urbani, L., Forty, E., Chambers, R., Longo, R., Olivo, A., and Endrizzi, M., "Monochromatic Propagation-Based Phase-Contrast Microscale Computed-Tomography System with a Rotating-Anode Source," *Phys. Rev. Applied* **11**, 034004 (Mar. 2019).

[5] Vittoria, F. A., Endrizzi, M., Diemoz, P. C., Wagner, U. H., Rau, C., Robinson, I. K., and Olivo, A., "Virtual edge illumination and one dimensional beam tracking for absorption, refraction, and scattering retrieval," *Appl. Phys. Lett.* **104**, 134102 (Mar. 2014).

[6] Vittoria, F. A., Kallon, G. K. N., Basta, D., Diemoz, P. C., Robinson, I. K., Olivo, A., and Endrizzi, M., "Beam tracking approach for single–shot retrieval of absorption, refraction, and dark–field signals with laboratory x–ray sources," *Appl. Phys. Lett.* **106**, 224102 (June 2015).

[7] Vittoria, F. A., Diemoz, P. C., Endrizzi, M., Rigon, L., Lopez, F. C., Dreossi, D., Munro, P. R. T., and Olivo, A., "Strategies for efficient and fast wave optics simulation of coded-aperture and other x-ray phase-contrast imaging methods," *Appl. Opt., AO* **52**, 6940–6947 (Oct. 2013).

[8] Massimi, L., Buchanan, I., Astolfo, A., Endrizzi, M., and Olivo, A., "Fast, non-iterative algorithm for quantitative integration of X-ray differential phase-contrast images," *Opt. Express, OE* **28**, 39677–39687 (Dec. 2020).